

# Report on progress in measuring $\beta$ -particle energies from Sr-90 emissions

Griffin Kowash

December 2020

## Contents

<b>1 Abstract</b>	<b>1</b>
<b>2 Introduction</b>	<b>2</b>
<b>3 Background</b>	<b>2</b>
<b>4 Cloud chamber</b>	<b>2</b>
4.1 Description . . . . .	2
4.2 Preliminary Results . . . . .	3
4.3 Flaws . . . . .	3
4.4 Improvements . . . . .	7
<b>5 Magnetic field</b>	<b>7</b>
5.1 Design . . . . .	7
5.2 Sensor . . . . .	9
<b>6 Radiation source</b>	<b>10</b>
<b>7 Energy measurement</b>	<b>12</b>
<b>8 Conclusion and Future Work</b>	<b>12</b>

## 1 Abstract

This report details current progress in an effort to characterize the beta spectrum of strontium-90 using a cloud chamber. Preliminary images of particle tracks from the cloud chamber are presented, and improvements for the design are discussed. A numerical model of the proposed field configuration is used to simulate particle tracks at different energies. The magnetic field sensor is demonstrated by measuring the field around a refrigerator magnet. The radiation source and energy measurement procedure are briefly discussed. Finally, plans for future work on this project are summarized.

## 2 Introduction

The cloud chamber was one of the earliest tools used to directly study subatomic particles. Cloud chambers played an important role in the first several decades of twentieth-century physics, such as in the discovery of the positron. While physicists later developed more effective devices such as bubble chambers and modern particle detectors, cloud chambers are still popular among educators and hobbyists due to their simple construction and visually striking results.

This experiment aims to go beyond qualitative observations and use a cloud chamber to characterize the beta-decay spectrum of radioactive strontium-90. Using magnets to curve the particle tracks and an overhead camera to measure the curvature, the energy of an electron emitted through beta decay can in principle be calculated. In practice, there are numerous complications that make this process more difficult. This report describes the current state of the experiment, presents simulations and preliminary measurements, and discusses plans for future work on the project.

## 3 Background

An electron moving through a magnetic field experiences a deflection due to the Lorentz force:

$$\vec{F} = q\vec{v} \times \vec{B} \quad (1)$$

If the magnetic field is constant and perpendicular to the direction of motion, it causes the particle to travel in a circle with a radius given by

$$r = \frac{mv}{qB} \quad (2)$$

If the radius of curvature is measured and the field strength is known, this equation can be rearranged to solve for the particle's velocity, and by extension its energy.

As discussed below, this experiment uses a non-uniform field, meaning that particle tracks will not curve circularly. Instead, the final analysis will calculate the expected trajectory of a given particle through the field for different energies and fit the simulation to match the observed track.

## 4 Cloud chamber

### 4.1 Description

The cloud chamber, shown in Figure 1, consists of 4 glass walls arranged in a square and fixed to a thin steel plate. During operation, the chamber is placed on top of a Styrofoam reservoir containing crushed dry ice, and a Styrofoam sheath is placed around the perimeter for additional insulation. The lid consists of a glass plate covered in black felt on one side, with a circle removed from

the middle to allow for overhead filming of particle tracks. To create the vapor cloud, 99% isopropyl alcohol is liberally applied to the felt and the lid is placed, felt side down, over the chamber.



Figure 1: Photo of cloud chamber used in the experiment, with ruler for scale.

As the alcohol evaporates, room-temperature vapor sinks toward the bottom of the chamber until it reaches the steel plate, which is cooled by dry ice. Upon cooling, the vapor condenses into a supersaturated cloud of droplets. Once a substantial cloud has formed, charged particles traveling through the supersaturated region will trigger condensation along their paths, making their trajectories visible to the observer.

## 4.2 Preliminary Results

Figures 2, 3, 4, 5, and 6 show a selection of particle tracks captured by the overhead camera. A refrigerator magnet placed on the floor of the chamber is visible in most of the images, although it had no visible effect on particle trajectories. A number of factors caused the tracks to appear very faint in the video, making automated image analysis impractical. Possible causes and solutions for this problem are discussed below.

While some distortion is present in the track geometries due to a persistent flow of air toward the top-left corner, several of the images, such as Figures 2 and 5, appear to clearly show beta particles scattering in the air.

## 4.3 Flaws

A number of flaws in the chamber made capturing reliable images of particle tracks difficult. One of the most significant issues is a leak in the contact between the glass wall and the metal base plate. This causes the vapor cloud to flow toward the leak, which is visible in the video as a persistent migration of the droplets toward the top-left of the frame.

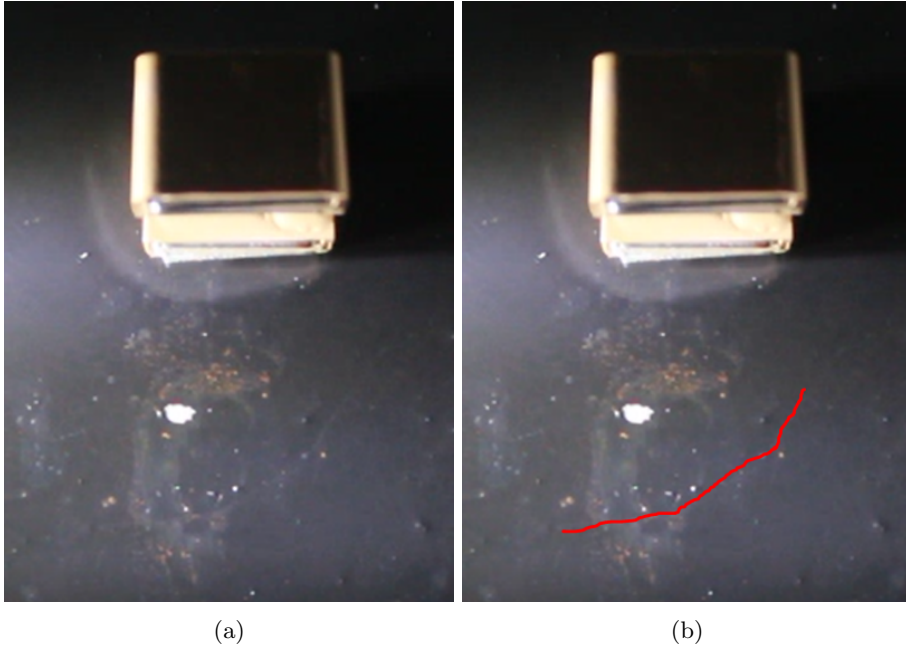
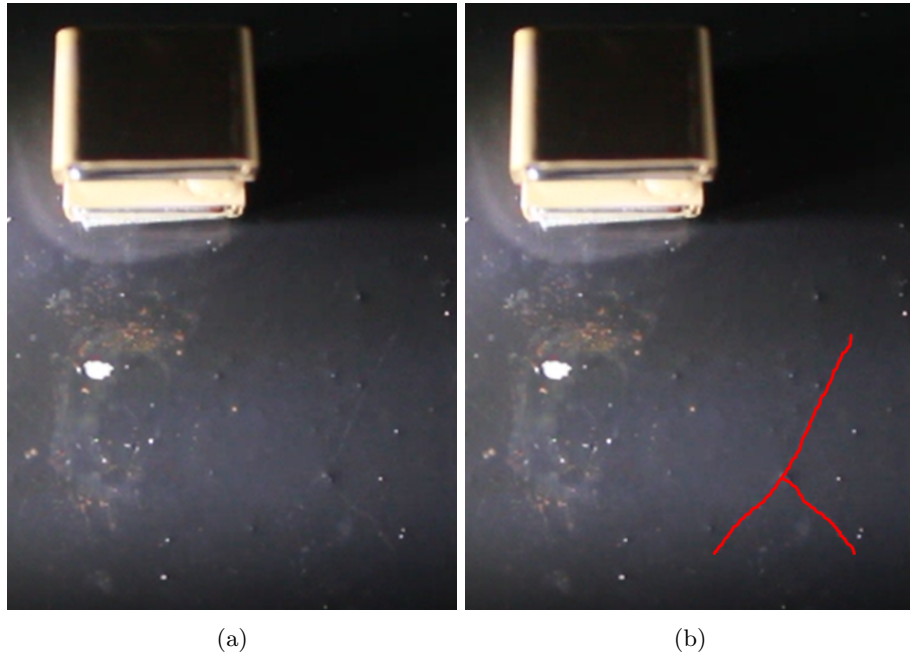


Figure 2: Image of suspected beta track. a) Original image and b) image with track marked in red. (Timestamp 6:11 in [video](#))

Because tracks may take up to a second to fully consolidate, this flow significantly disrupts the shape of the tracks. Due to problems with the lighting discussed below, tracks are often not visible to the camera until they have fully consolidated, making it difficult to extract reliable trajectories from the video footage. The outflow may also reduce the concentration of alcohol in the super-saturated layer, resulting in thinner, less visible tracks.

This leak has two major causes: distortion of the plate due to cooling and corrosion of the metal. The plate is roughly 0.5mm thick, and cooling from the dry ice causes it to bow as it contracts. In addition, because the chamber was constructed several years before, corrosion of the metal has weakened the silicone contacts between the glass and the base plate. As a result, the contraction of the metal tends to break the contact in one corner of the chamber, allowing vapor to escape during operation. Attempts to fill the gap have reduced the problem, but they have not been fully successful.

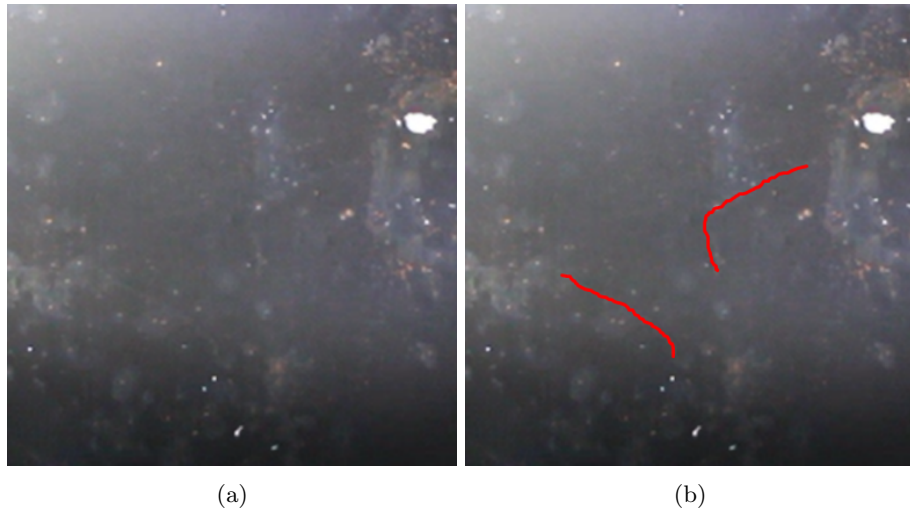
Another flaw in the chamber design relates to the lighting. To make the tracks visible, it is crucial to strongly light the vapor layer while reducing glare off the base plate as much as possible. This is best achieved with a strong light source aimed horizontally through the side of the layer. Unfortunately, the design of the chamber prevents this, because the silicone and plastic layer used to join the glass to the base plate obstructs the lowest 2cm of the wall. Instead, a flashlight is angled slightly downward from above this layer, which



(a)

(b)

Figure 3: Image of suspected beta track. a) Original image and b) image with track marked in red. (Timestamp 6:24 in [video](#))



(a)

(b)

Figure 4: Image of two suspected beta tracks. a) Original image and b) image with tracks marked in red. Curvature is likely an artifact of airflow toward the top-left corner. (Timestamp 6:25 in [video](#))

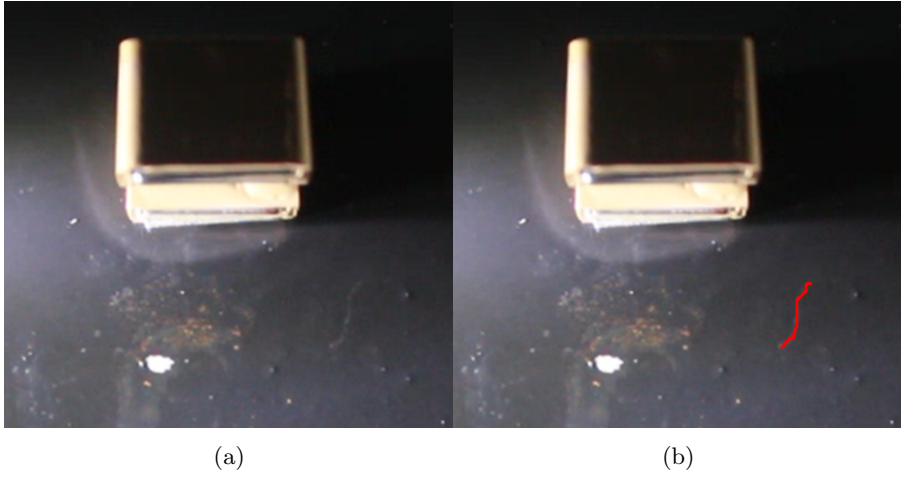


Figure 5: Image of unidentified particle track. a) Original image and b) image with track marked in red. (Timestamp 6:18 in [video](#))



Figure 6: Image of unidentified particle track. a) Original image and b) image with track marked in red. (Timestamp 9:10 in [video](#))

both increases the amount of glare off the base plate and reduces the illuminated area.

Finally, because this experiment requires the use of precisely known magnetic fields, the ferromagnetic nature of the metal base is likely a problem. While the effects of its magnetization have not been characterized, it introduces an additional source of error that would make the final analysis more difficult.

## 4.4 Improvements

Given the flaws described above, the best option for future work is to construct an entirely new cloud chamber. The new chamber should have a much thicker base plate to reduce bowing, in the range of a few millimeters, and it should be composed of aluminum or stainless steel to reduce magnetization. The body of the chamber should be replaced by a solid plastic or glass container, like a small fish tank or terrarium bin. To eliminate air leakage, the lip of the container should be lubricated and pressed into a thick layer of silicone sealant on the base plate, creating a smooth seal into which the container can be fit during use.

Lighting can be improved by installing a strip of bright LEDs on the inside or outside edge of the chamber, with a shield on the top and bottom to reduce the amount of light straying from the plane of the vapor layer. Including some form of control over the brightness and number of active LEDs may be useful for fine-tuning the lighting during operation. Finally, while the original base plate was painted matte black to reduce specular reflection, reducing diffuse reflection by using a glossy paint might function better to improve image quality.

An additional route for improving the image quality may be creating an electric field within the vapor layer. This reportedly serves to increase the thickness of tracks, which would make capturing them on camera easier. Figure 7 shows an image from a test two years prior in which a "bug zapper" power supply was used to create an electric field within the chamber. The observed tracks were noticeably thicker; however, the effect of an external electric field on particle trajectories has not yet been explored for this experiment.

## 5 Magnetic field

### 5.1 Design

In accordance with the energy and curvature calculations described in the Background section, the simplest approach would be to create a uniform magnetic field within the vapor layer. This is the route taken in Welch 2012 [1], which uses a Helmholtz coil encircling the cloud chamber to create a uniform field. However, this approach requires high currents and large amounts of magnet wire, which is both cost-prohibitive and infeasible for an at-home experiment. In addition, the setup described in the paper yielded fairly weak magnetic fields of about 5mT. A weaker field causes less curvature, and given the limited distance an electron can travel through air, this reduces the amount of measurable deflection.

This experiment sacrifices field uniformity in favor of stronger fields and more accessible materials by using permanent magnets to induce curvature in the particle tracks. The selected neodymium magnets have dimensions 5.08cm x 2.54cm x 1.27cm and magnetization 1.35T. They will be arranged in pairs joined along the longest axis, with the two pairs oriented parallel to each other and separated by about 10cm, as shown in Figure 8.



Figure 7: Image of particle tracks with an electric potential on the order of 100V between the top and bottom of the chamber.

This configuration creates a field that varies between around 30mT in between the two magnet blocks to around 100mT toward the edge. Crucially, the dimensions help minimize the horizontal components of the magnetic field within the central region, which reduces the impact of uncertainty in particle track height. Otherwise, any horizontal component will cause the particle to deflect upward or downward, which will interfere with accurate measurement of the energy.

Due to the non-uniform magnetic field, particle tracks will not be circular, but a rough measure of their curvature can be found by selecting three points  $x$ ,  $y$ , and  $z$  along the track and calculating the Menger curvature as follows:

$$c(x, y, z) = \frac{2 \sin(\angle xyz)}{|x - z|} \quad (3)$$

where  $\angle xyz$  is the angle subtended by the three points, and  $|x - z|$  is the distance between the first and last points. The calculated curvature depends on the energy of the incoming particle as well as the particular points selected along the trajectory, but radii for the configuration described above typically range between 2cm and 5cm. Having a small radius of curvature is important to obtain measurable results, because collisions with air molecules limit the distance a beta particle can travel through air.

The calculation used for the track simulations only considers the Lorentz force, and neglects the interaction between the non-uniform field and the electron magnetic moment. To justify ignoring this effect, the dipole force can be

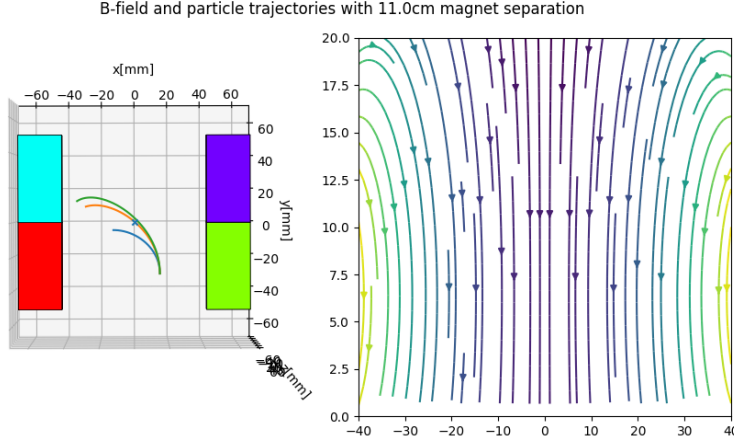


Figure 8: Left: Overhead view of particle track simulation for energies of 0.1MeV (blue), 0.5MeV (orange), and 2.4MeV (green). Right: Magnetic field lines along a slice parallel to the xz-plane through the center of the configuration.

calculated using the following equation:

$$\vec{F}_d = \vec{\nabla}(\vec{\mu} \cdot \vec{B}) \quad (4)$$

Comparing a point halfway between the two magnets to a point halfway toward one side (a distance of about 2.5cm for a 10cm magnet separation) gives values of 32mT and 98mT in the vertical direction, respectively, corresponding to an average gradient of 0.24 T/m. Using the electron magnetic moment of  $\mu_e = -9.28 \times 10^{-24}$  J/T gives a force on the order of  $10^{-24}$  N. In comparison, the Lorentz force for an electron in this experiment is typically on the order of  $10^{-12}$  and seldom less than  $10^{-14}$ , so the contribution from the dipole moment is insignificant.

## 5.2 Sensor

The Vernier Go Direct 3-Axis magnetic field sensor used in this experiment measures magnetic fields up to 130mT in three dimensions with 0.1mT uncertainty. While the neodymium magnets used for this experiment were not available at the time of writing, the sensor was used to characterize the magnetic field of a refrigerator magnet. The resulting direction field is depicted in Figure 9 to scale, with the magnet overlaid to show the physical location of the points measured.

Based on the direction field, it is apparent that upper magnet in each pair has a south pole on the left edge, as the fields point strongly inward at both locations. The magnetization geometry of the lower magnet in each pair is less clear; the north-south axis may be rotated 90° relative to the upper magnet, or the poles may be on the faces instead of the edges.

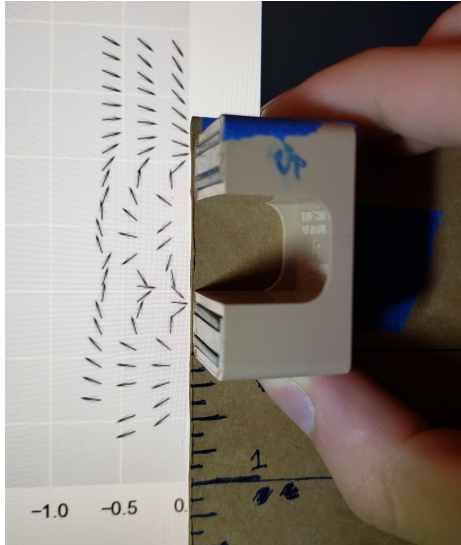


Figure 9: Measured field of the refrigerator magnet plotted to scale, with the magnet overlaid to show the physical locations of the field points. The object consists of two closely-spaced pairs of magnets separated by a gap of a couple centimeters.

Figure 10 shows the total field strength in the y-direction (moving upward in the reference frame of Figure 9), with the sensor moving along a line directly in front of the magnets. The plot shows a maximum field strength of about 28mT, with the two peaks corresponding to the two magnet pairs.

A major task in the future of this experiment will be to measure the field created by the proposed magnet configuration and compare it to the theoretical model (Figure 8). If the measurements conflict with the model, the model will either need to be adjusted or replaced entirely with measured values, which would introduce significant error.

## 6 Radiation source

The proposed radiation source for this experiment is a  $0.1 \mu\text{Ci}$  disk of strontium-90. The source was not available at the time of writing, but it will provide a much more reliable way to test the cloud chamber, as the origin and direction of background radiation is random. The beta spectrum of the Sr-90/Y-90 decay channel peaks at about 0.7MeV and falls to zero by 2.4MeV [2].

In order to restrict particles to the horizontal plane, it will be necessary to include some shielding in front of the source. This will limit the uncertainty in the vertical position and velocity components, but with the consequence of restricting the rate of detectable events. Future work will require determining

Total field strength vs y-position (0cm separation from magnet)

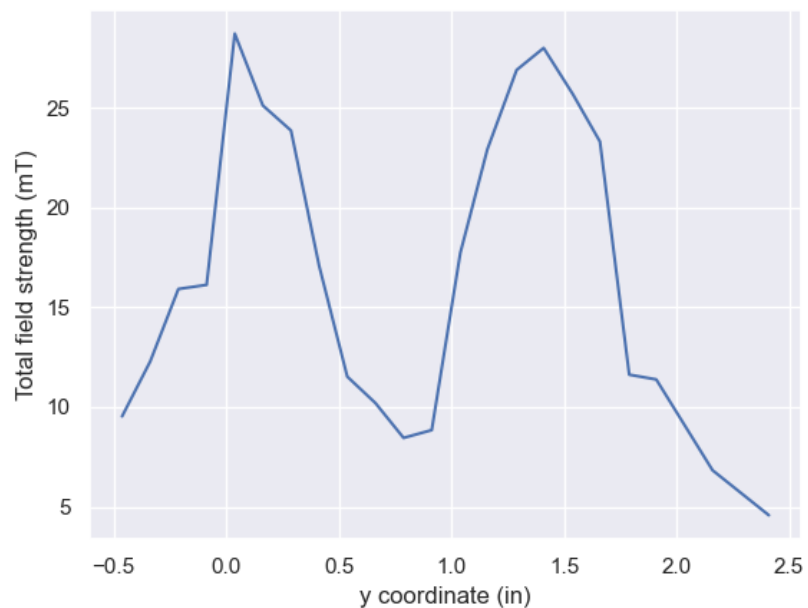


Figure 10: Total field strength plotted against y coordinate (up-direction), with a 0cm separation between the sensor and the magnet edge.

the best trade-off between event frequency and uncertainty in initial position and velocity direction.

## 7 Energy measurement

The exact method for energy measurement is currently undecided, as it will depend strongly on the quality of the final track images. One method under consideration is a semi-manual process in which the experimenter manually selects two points adjacent points near the origin of a track, which gives the program the particle's initial position and velocity direction. The program uses that information to simulate a 0.5MeV particle and overlays its trajectory on the image. The experimenter compares the observed and simulated tracks and uses the keyboard's arrow keys to adjust the parameters until the nearest match is found.

A preliminary test of this method using simulated particle tracks has yielded encouraging results, with particle energies correctly estimated to within 0.1MeV. Designing a reliable procedure to achieve accurate alignment between the cloud chamber image and the simulated field is critical to improve the results. In addition, further investigation is needed to determine the degree of error introduced by uncertainty in the initial height and velocity vector of the particle.

## 8 Conclusion and Future Work

The project will be continued with the goal of obtaining presentable results in time for the spring 2021 senior seminar presentations. There are several important steps that need to be taken to achieve this.

First, it will be important to construct a new chamber with a more secure seal and better lighting system. Creating thick, well-lit tracks visible to the overhead camera is essential for the experiment, especially if the image analysis will ultimately be automated.

Second, the magnet configuration will need to be characterized as precisely as possible. This will help confirm or contradict the theoretical model presented above. Accurate knowledge of the field is critical for obtaining useful energy estimates.

Third, the nature of the radioactive source must be studied in the cloud chamber in order to design an effective shield to restrict the initial vertical position and velocity vector. If the event rate is high, a more restrictive shield will be possible, reducing uncertainty in the final calculations.

Fourth, a method for image analysis and energy estimation must be designed, with both accuracy and efficiency taken into consideration. Fully automating the process would allow for a much larger sample size and more robust results, but depending on the final image quality, a semi-manual process as described above may be more reliable.

Finally, a thorough error analysis must be performed, taking into account uncertainties in field strength and position measurements, initial positions and velocity vectors of particles, and other factors. Characterizing the uncertainty is important to determine whether or not the final results agree with the accepted beta spectrum of the source.

## References

- [1] Welch, Alex. Diffusion Cloud Chamber. Menlo School Roundtable, Fall 2012. [https://roundtable.menloschool.org/issue13/6\\_Welch\\_MS\\_Roundtable\\_13\\_Fall\\_2012.pdf](https://roundtable.menloschool.org/issue13/6_Welch_MS_Roundtable_13_Fall_2012.pdf)
- [2] Laoues, Mostafa et. al. Comparison between beta radiation dose distribution due to LDR and HDR ocular brachytherapy applicators using GATE Monte Carlo platform. *Physica Medica*, 32(8). August 2016. [https://www.researchgate.net/figure/The-energy-spectrum-of-90-Sr-90-Y\\_fig1\\_305922539](https://www.researchgate.net/figure/The-energy-spectrum-of-90-Sr-90-Y_fig1_305922539)
- [3] Kowash, Griffin. Cloud chamber test. December 2020. <https://youtu.be/TQPKi41fzPg>